

Transferred charge analysis of evaporated ZnS:Mn alternating-current thin-film electroluminescent devices

R. Myers and J. F. Wager

Department of Electrical and Computer Engineering, Center for Advanced Materials Research, Oregon State University, Corvallis, Oregon 97331-3211

(Received 23 September 1996; accepted for publication 4 October 1996)

Evaporated ZnS:Mn alternating-current thin-film electroluminescent (ACTFEL) devices are assessed via frequency- and temperature-dependent transferred charge analysis. The frequency-dependent trends involve the threshold voltage and the slope of the transferred charge immediately above threshold, both of which increase with increasing frequency. At ~ 15 – 20 V above threshold, the slope of the transferred charge curve is relatively independent of frequency and is approximately equal to the physical insulator capacitance. The temperature-dependent trends indicate that the phosphor capacitance increases and the slope of the transferred charge immediately above threshold decreases with increasing temperature. These frequency- and temperature-dependent trends are interpreted as arising from metastable hole trapping in which holes created in the phosphor by band-to-band impact ionization remain trapped in metastable traps at the cathode interface instead of being annihilated by electrons trapped at interface states. © 1997 American Institute of Physics. [S0021-8979(97)08001-8]

I. INTRODUCTION

In 1990, Bringuier¹ applied transferred charge analysis to the problem of electron multiplication in ZnS:Mn alternating-current thin-film electroluminescent (ACTFEL) devices. In this study, Bringuier deduced that a metastable hole trap must exist (he referred to this as slow hole trapping) and that electron multiplication must be operative in order to explain anomalously steep transferred charge characteristics. Subsequently, we concluded² from several different experimental studies and from various observations that electron multiplication by band-to-band impact ionization occurs in evaporated ZnS:Mn ACTFEL devices. Furthermore, in order to interpret and simulate measured transferred charge trends we also needed to invoke the existence of Bringuier's metastable hole trap.

The purpose of the work described herein is to present a study in which the frequency and temperature dependence of transferred charge characteristics of evaporated ZnS:Mn ACTFEL devices are monitored. These frequency- and temperature-dependent characteristics are then interpreted in terms of metastable hole trapping. It should be noted that two unconventional procedures for accomplishing transferred charge analysis are employed in this study; the primary reason that these procedures are unconventional relates to the fact that two kinds of offset adjustment procedures are implemented, as described in the following.

II. EXPERIMENTAL PROCEDURE

A. ACTFEL samples and general procedures

The ACTFEL devices used in this study are fabricated at Planar America. They consist of an evaporated ZnS:Mn active phosphor layer sandwiched between two sputtered silicon oxynitride layers. Contacts are made of aluminum and indium-tin oxide (ITO).

The electrical analysis is accomplished using a conventional electrical test circuit³ consisting of an arbitrary wave form generator (Wavetek Model 395) in conjunction with a high-voltage amplifier to generate the bipolar pulse wave form that drives a series resistor (R_s), the ACTFEL device, and a sense capacitor (C_s). For these experiments, $R_s = 500 \Omega$ and $C_s = 110.8$ nF. The instantaneous voltage across the ACTFEL device [$v_{EL}(t)$] and the instantaneous external charge [$q_{ext}(t) = C_s v_{sense}(t)$] are obtained using a digitizing oscilloscope (Tektronix Model TDS 420A). The wave form employed is comprised of symmetric bipolar voltage pulses with $5 \mu s$ rise and fall times and a $30 \mu s$ pulse width; the maximum applied voltage (V_{max}) and the frequency of the wave form are varied for the work described herein. Note that a change in the wave form frequency changes only the separation between voltage pulses.

For temperature-dependent studies, the ACTFEL device is placed in an environment chamber (Sun System Model EC1A), which provides a dry nitrogen atmosphere, as well as temperature control. Device temperatures are measured by a thermocouple in contact with the ACTFEL glass substrate.

Prior to electrical analysis the ACTFEL device is aged for 1 h at a temperature of $73^\circ C$, a frequency of 3 kHz, and an overvoltage of 30 V. The electrical characteristics do not appear to change noticeably with time after the ACTFEL device is subjected to this aging procedure.

B. Maximum charge–maximum applied voltage analysis

The two transferred charge analysis techniques employed in this study are denoted maximum charge–maximum applied voltage ($Q_{max} - V_{max}$) and external maximum charge–maximum applied voltage ($Q_{max}^e - V_{max}$) measurements. The $Q_{max} - V_{max}$ measurement has been described previously.² However, note that the $Q_{max} - V_{max}$ measurement procedure employed in the present study differs

from that described previously in that an offset adjustment procedure is used, as described in the following. The $Q_{\max}^e - V_{\max}$ technique is identical to a conventional transferred charge measurement (in the literature this measurement is sometimes referred to as a $\Delta Q - V$ measurement^{4,5}) except for the fact that an offset adjustment procedure is used.

Offset adjustment is a procedure in which each $q_{\text{ext}}(t)$ and $v_{\text{EL}}(t)$ transient curve is individually offset adjusted prior to being further processed in order to accomplish a $Q_{\max} - V_{\max}$ or $Q_{\max}^e - V_{\max}$ measurement.

The idea underlying offset adjustment of the $q_{\text{ext}}(t)$ curve⁶ is that this curve may be asymmetrically displaced from the origin of the voltage axis. Such an asymmetric displacement of the $q_{\text{ext}}(t)$ curve from the voltage axis origin is referred to as $q_{\text{ext}}(t)$ offset. A $q_{\text{ext}}(t)$ offset yields charge–voltage ($Q - V$) curves that are displaced vertically above or below the voltage axis and internal charge–phosphor field ($Q - F_p$) curves that are displaced laterally above or below the phosphor field axis.⁶ Our procedure for $q_{\text{ext}}(t)$ offset adjustment is to simply displace the $q_{\text{ext}}(t)$ curve until it is symmetrically positioned above the voltage axis origin [i.e., the points of a $q_{\text{ext}}(t)$ curve corresponding to the onset of the positive and negative voltage pulses (these points are often labeled A and F in the literature^{3,6}) are symmetrically positioned about the voltage origin]. The amount of voltage shift that is required to symmetrically displace the $q_{\text{ext}}(t)$ curve is recorded and is regarded as a measure of the extent of the $q_{\text{ext}}(t)$ offset. Simulation indicates⁶ that $q_{\text{ext}}(t)$ offset may arise from an asymmetry in the interface state depths at the two phosphor/insulator interfaces or from an asymmetry in the location of space charge generation in the phosphor.

The second kind of offset procedure that we employ is to monitor $v_{\text{EL}}(t)$ and to reset the base line of $v_{\text{EL}}(t)$ to ensure that the base line occurs at zero volts. We find that $v_{\text{EL}}(t)$ curves typically require an offset adjustment of $\sim 1\% - 3\%$ of V_{\max} due to small and random offset inaccuracies in the oscilloscope. $v_{\text{EL}}(t)$ offset is manifest in a $Q - V$ curve as a displacement of the leakage charge off of the charge axis.

A $Q_{\max}^e - V_{\max}$ curve is generated as follows. Sets of $q_{\text{ext}}(t)$ and $v_{\text{EL}}(t)$ curves are obtained as a function of V_{\max} and are individually offset adjusted. Subsequently, a sorting routine is invoked to determine the maximum $q_{\text{ext}}(t)$ value, corresponding to Q_{\max}^e , and the maximum $v_{\text{EL}}(t)$ value, corresponding to V_{\max} . Finally, these Q_{\max}^e and V_{\max} sets are plotted to obtain a $Q_{\max}^e - V_{\max}$ curve. A $Q_{\max} - V_{\max}$ curve is obtained in an identical manner except that after $q_{\text{ext}}(t)$ offset adjustment is accomplished, the internal charge transient [$q(t)$] is evaluated using the following transformation equation:^{3,7}

$$q(t) = \frac{(C_i + C_p)}{C_i} q_{\text{ext}}(t) - C_p v_{\text{EL}}(t), \quad (1)$$

and then $q(t)$ is used instead of $q_{\text{ext}}(t)$.

Note that the evaporated ZnS:Mn ACTFEL devices investigated in this study do not exhibit a large amount of $q_{\text{ext}}(t)$ offset. This is not surprising since the electrical characteristics of these devices are known to be symmetric^{8,9} and

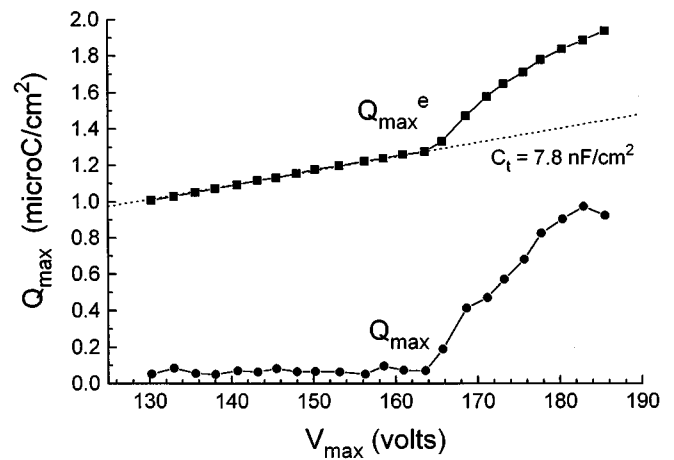


FIG. 1. Comparison of a $Q_{\max} - V_{\max}$ and a $Q_{\max}^e - V_{\max}$ curve for an evaporated ZnS:Mn ACTFEL device measured at room temperature and at a frequency of 1000 Hz.

there is no evidence for dynamic space charge generation in these devices.²

III. EXPERIMENTAL RESULTS AND DISCUSSION

A. A comparison of $Q_{\max} - V_{\max}$ and $Q_{\max}^e - V_{\max}$ analysis

Figure 1 shows a comparison of $Q_{\max} - V_{\max}$ and $Q_{\max}^e - V_{\max}$ curves obtained at room temperature (300 K) and at an applied frequency of 1000 Hz. From either of these curves it is easy to determine that the threshold voltage (V_{th}) is approximately 164 V. Furthermore, the slope of the $Q_{\max}^e - V_{\max}$ curve prior to threshold is equal to 7.8 nF/cm², which corresponds to the total capacitance (C_t) of the ACTFEL device.

A comparison of the two curves shown in Fig. 1 indicates that there is distinctly more noise in the $Q_{\max} - V_{\max}$ curve. The source of this increased noise is apparent from an analysis of Eq. (1); $q(t)$ noise (and, hence, Q_{\max} noise) is comprised of noise arising from both $q_{\text{ext}}(t)$ and $v_{\text{EL}}(t)$ data sets. Moreover, since the Q_{\max} and the V_{\max} noise both depend upon the $v_{\text{EL}}(t)$ noise, the Q_{\max} noise and the V_{\max} noises are correlated in a $Q_{\max} - V_{\max}$ curve. Since, in a $Q_{\max}^e - V_{\max}$ curve there is less noise, the noise is uncorrelated, and since C_t may be evaluated directly, we will exclusively use $Q_{\max}^e - V_{\max}$ curves in the remainder of this paper and will no longer consider $Q_{\max} - V_{\max}$ analysis.

Figure 2 is a plot of several $Q_{\max}^e - V_{\max}$ curves obtained for an evaporated ZnS:Mn ACTFEL device measured at a temperature of 100 K and at frequencies of 100, 300, 1000, 2000, and 3000 Hz. Additionally, a dotted curve indicating the insulator capacitance is shown above threshold in Fig. 2. Several trends are evident from Fig. 2. First, the threshold voltage decreases as a function of increasing frequency. Second, the initial slope of each $Q_{\max}^e - V_{\max}$ curve just beyond threshold is greater for increasing frequency. Third, the slopes of each $Q_{\max}^e - V_{\max}$ curve at overvoltages in excess of $\sim 15 - 20$ V above threshold become relatively constant and are approximately equal to the insulator capacitance.

In order to examine the trends of Fig. 2 in more detail, differentiated $Q_{\max}^e - V_{\max}$ curves (i.e., dQ_{\max}^e/dV_{\max}) are plot-

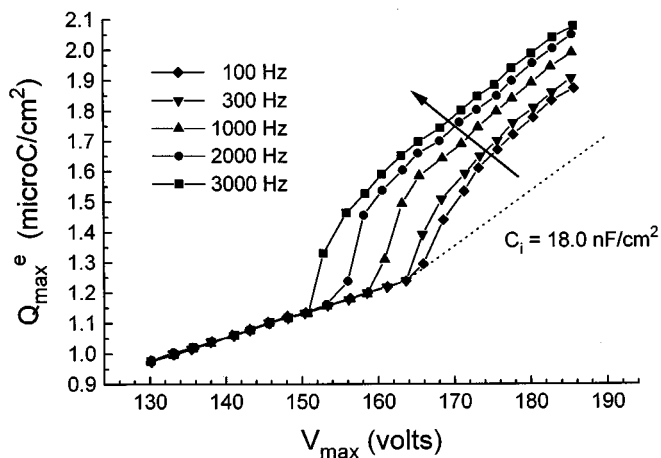


FIG. 2. $Q_{\max}^e - V_{\max}$ curves for an evaporated ZnS:Mn ACTFEL device measured at a temperature of 100 K and at frequencies of 100, 300, 1000, 2000, and 3000 Hz. The arrow indicates the trend in terms of increasing frequency.

ted as a function of V_{\max} in Fig. 3. Note that differentiation amplifies the detailed features of the trends shown in Fig. 2 so that they are more readily apparent. Additionally, the differentiated $Q_{\max}^e - V_{\max}$ curves may be readily interpreted as capacitances; recognizing this, the total and insulator physical capacitances are also indicated in Fig. 3. The same three trends as discussed with respect to Fig. 2 also apply to Fig. 3. First, the threshold voltage decreases with increasing frequency. Second, the amount of overshoot in the differentiated $Q_{\max}^e - V_{\max}$ curves shown in Fig. 3 (corresponding to the slope of the $Q_{\max}^e - V_{\max}$ curves just beyond threshold, as shown in Fig. 2) is greater for increasing frequency. Third, note that above ~ 15 – 20 V beyond threshold the differentiated $Q_{\max}^e - V_{\max}$ curves all approach the physical insulator capacitance.

The frequency-dependent trends evident in Figs. 2 and 3 are interpreted in terms of metastable hole trapping, as pro-

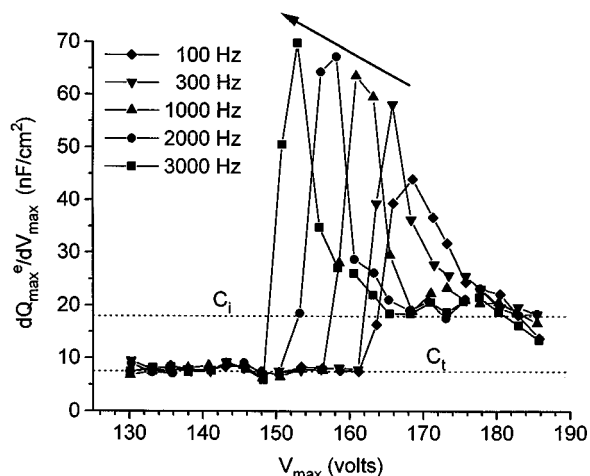


FIG. 3. Differentiated $Q_{\max}^e - V_{\max}$ curves for an evaporated ZnS:Mn ACTFEL device measured at a temperature of 100 K and at frequencies of 100, 300, 1000, 2000, and 3000 Hz. The arrow indicates the trend in terms of increasing frequency.

posed previously.^{1,2} The idea of metastable hole trapping is envisaged as follows. When an evaporated ZnS:Mn ACTFEL device is subject to an applied voltage pulse of sufficient magnitude to result in the flow of conduction charge, the phosphor field is sufficiently large (at least near the cathode interface) that holes are created via band-to-band impact ionization. These holes then drift to the cathode interface in a very short time (\sim ps). Once these holes reach the cathode interface, they are trapped in metastable hole traps. These hole traps are metastable because, given sufficient time, these trapped holes will be annihilated via recombination with electrons trapped in interface states. However, the time it takes to annihilate these metastable holes via interface state electron trapping is very long [it has been estimated to be ~ 1.2 ms (Ref. 2)] compared to the microsecond time scale of the applied voltage wave form pulses.

The three trends indicated in Figs. 2 and 3 may be explained by invoking the metastable hole trapping model. When metastable hole trapping occurs, the slope in a $Q_{\max}^e - V_{\max}$ curve just above threshold is greater than C_i (Fig. 2) or, equivalently, overshoot exists in a differentiated $Q_{\max}^e - V_{\max}$ curve (Fig. 3) since more electrons occupy interface states in a nonsteady-state manner than if steady state were to occur; steady state would be established if all of the holes trapped at the cathode interface were annihilated by interface state electrons. If more electrons occupy interface states in a nonsteady-state manner, these electrons contribute an increased amount of conduction charge compared to that expected if steady state were to prevail; an increased amount of conduction charge for the same amount of applied voltage translates into an increase in dQ_{\max}^e/dV_{\max} in excess of C_i , as observed in Fig. 3. According to the metastable hole trapping model, the frequency dependence of the threshold voltage (Figs. 2 and 3), the frequency dependence of the slope of the $Q_{\max}^e - V_{\max}$ curve just above threshold (Fig. 2), and the frequency dependence of the overshoot of the differentiated $Q_{\max}^e - V_{\max}$ curve (Fig. 3) are simply attributed to the fact that more metastable holes are available at the onset of a voltage pulse at higher frequencies because there is less time between voltage pulses for the metastable holes to be annihilated. The fact that the slope of a $Q_{\max}^e - V_{\max}$ curve (Fig. 3) or, equivalently, the overshoot in a differentiated $Q_{\max}^e - V_{\max}$ curve (Fig. 3) becomes relatively constant above ~ 15 – 20 V in excess of threshold is attributed to the fact that the majority of the conduction electrons at these overvoltages are being sourced from interface states that are normally occupied in steady state (i.e., at overvoltages in excess of ~ 15 – 20 V, a negligible fraction of the conduction electrons are sourced from interface states that are occupied in a nonsteady-state manner).

Further insight into the nature of these metastable hole traps is provided by Fig. 4, which is a plot of $Q_{\max}^e - V_{\max}$ curves measured at a frequency of 1000 Hz and temperatures of 100, 200, 300, and 400 K. The trends evident from Fig. 4 are that C_t increases, the threshold increases slightly, and the slope in the $Q_{\max}^e - V_{\max}$ curve just above threshold decreases with increasing temperature. The temperature dependence of the threshold voltage is unexpected and so its origin is further investigated in Table I where the threshold voltage (V_{th}),

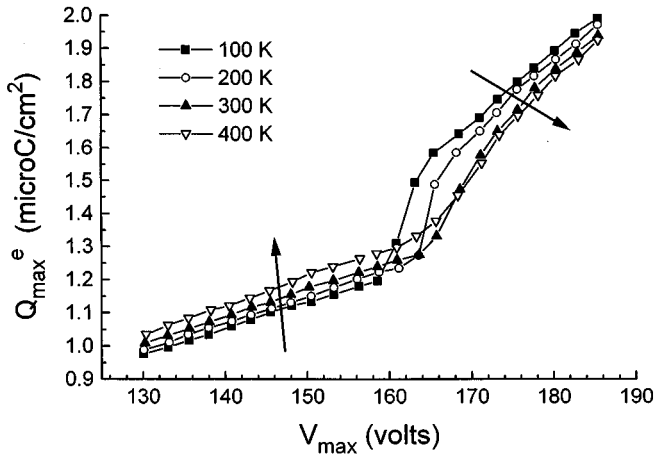


FIG. 4. $Q_{\max}^e - V_{\max}$ curves for an evaporated ZnS:Mn ACTFEL device measured at a temperature of 100 K and at frequency of 1000 Hz and at temperatures of 100, 200, 300, and 400 K. The arrows indicate the trend in terms of increasing temperature.

the total capacitance (C_t), the phosphor capacitance (C_p), and the phosphor threshold field (F_p^{th}) are all tabulated as a function of temperature for the curves shown in Fig. 4. V_{th} and C_t are measured quantities. C_p and F_p^{th} are calculated assuming that C_i is temperature independent. [Capacitance–voltage ($C-V$) measurements indicate that C_p changes much more with temperature than C_i ; thus, the temperature dependence of C_t is attributed exclusively to C_p .] With the assumption that C_i is temperature independent, Table I indicates that, to within experimental error, E_p^{th} is constant and is not temperature dependent. This temperature independence of F_p^{th} is consistent with tunnel emission as the dominant mechanism of electron injection from interface states, since tunneling is temperature independent. This is consistent with current thinking about the device physics operation of evaporated ZnS:Mn ACTFEL devices.⁵ Therefore, we conclude from Table I that the temperature dependence of the threshold voltage arises exclusively from the temperature dependence of the phosphor capacitance.

The last Fig. 4 trend that needs to be discussed is the temperature dependence of the slope of $Q_{\max}^e - V_{\max}$ curves. In terms of the metastable hole trap model, we interpret this trend as evidence that the annihilation of metastable hole traps is temperature dependent and that these metastable holes are more readily annihilated by interface state electrons at higher temperatures. This suggests that the annihilation of metastable hole traps does not involve pure tunneling from

TABLE I. Temperature dependence of the threshold voltage (V_{th}), the total capacitance (C_t), the phosphor capacitance (C_p), and the phosphor threshold field (F_p^{th}). C_p and F_p^{th} are calculated assuming that C_i is temperature independent.

Temperature (K)	V_{th} (V)	C_t (nF)	C_p (nF)	F_p^{th} (MV/cm)
100	158	7.50	12.9	1.53
200	164	7.65	13.3	1.57
300	166	7.80	13.8	1.57
400	166	8.00	14.4	1.54

interface state electrons since tunneling is known to be temperature independent. Perhaps metastable hole annihilation occurs via phonon-assisted tunneling since this process would be more effective at higher temperatures. More work is required to unequivocally identify the mechanism of metastable hole trap annihilation.

The physical nature of this metastable hole trap is currently unknown. The most likely physical mechanism that would be consistent with the metastable nature of such a trap is physical separation of the hole trap from the interface where the interface states are located so that the annihilation of the metastable hole by the interface electron is impeded because of the small amount of wave-function overlap occurring between these physically separated trapped charges. Again, more work is required before atomic identification of this metastable hole trap can be accomplished.

IV. CONCLUSIONS

Maximum charge–maximum applied voltage ($Q_{\max}^e - V_{\max}$) and external maximum charge–maximum applied voltage ($Q_{\max}^e - V_{\max}$) measurements as a function of frequency and temperature are used for the characterization of evaporated ZnS:Mn ACTFEL devices. The $Q_{\max}^e - V_{\max}$ method is preferred to the $Q_{\max} - V_{\max}$ method because of noise considerations and because of the extra information that is provided from the prethreshold displacement charge flow. Essentially, the $Q_{\max}^e - V_{\max}$ technique described in this paper is identical to standard transferred charge measurements except that the $q_{\text{ext}}(t)$ and $v_{\text{EL}}(t)$ curves are offset corrected when accomplishing $Q_{\max}^e - V_{\max}$ analysis.

The focus of the present study is with respect to the nature of the frequency and temperature dependencies of the $Q_{\max}^e - V_{\max}$ characteristics of evaporated ZnS:Mn ACTFEL devices. The frequency-dependent trends involve a decrease in the threshold voltage, increase in the slope of the $Q_{\max}^e - V_{\max}$ curve just above threshold, and a saturation in the slope of the $Q_{\max}^e - V_{\max}$ curve at voltages $\sim 15-20$ V above threshold with increasing frequency. The temperature-dependent trends involve an increase in the phosphor capacitance and a decrease in the slope of the $Q_{\max}^e - V_{\max}$ curve just above threshold with increasing temperature.

These frequency- and temperature-dependent $Q_{\max}^e - V_{\max}$ trends are attributed to metastable hole trapping at the cathode interface and to the rather sluggish kinetics of the annihilation of these metastable hole traps by interface state electrons. The physical nature of these metastable hole traps and of the mechanism of metastable hole trap annihilation are obscure at this time.

ACKNOWLEDGMENTS

The authors wish to thank Paul Keir and Robert Thuemler for useful discussions during the course of this work and to Sey-Shing Sun for providing samples. This work was supported by the U.S. Army Research Office under Contract No. DAAH04-94-G-0324 and by the Defense Advanced Research Projects Agency under the Phosphor Technology Center of Excellence, Grant No. MDA 972-93-1-0030.

- ¹E. Bringuiet, J. Appl. Phys. **67**, 7040 (1990).
- ²W. M. Ang, S. S. Pennathur, L. Pham, J. F. Wager, S. M. Goodnick, and A. A. Douglas, J. Appl. Phys. **77**, 2719 (1995).
- ³A. Abu-Dayah, S. Kobayashi, and J. F. Wager, J. Appl. Phys. **62**, 744 (1993).
- ⁴Y. A. Ono, H. Kawakami, M. Fuyama, and K. Onisawa, Jpn. J. Appl. Phys. 1 **26**, 1482 (1987).
- ⁵Y. A. Ono, *Electroluminescent Displays* (World Scientific, Singapore, 1995).
- ⁶S. Shih, P. D. Keir, J. Hitt, and J. F. Wager, Appl. Phys. Lett. **69**, 1921 (1996).
- ⁷E. Bringuiet, J. Appl. Phys. **66**, 1314 (1989).
- ⁸J. D. Davidson, S. Kobayashi, and J. F. Wager, J. Appl. Phys. **71**, 4040 (1992).
- ⁹J. D. Davidson, J. F. Wager, R. I. Khormaei, C. N. King, and D. Williams, IEEE Trans. Electron Devices **ED-39**, 1122 (1992).